PAPER

Check for updates

Designing a locally produced DENV-1 nucleic acid diagnostic for low resource regions with endemic disease

Adam Roberts,[a] Dushanth Seevaratnam,†[a] Ferguie B. Solis,[b] Maria Rhona G. Bergantin,[b] Dharmatov Rahula B. Albano, [iD][b] Fortunato B. Sevilla, III[b] and Elizabeth A. H. Hall [iD] *[a]

Using recombinant techniques, to support local production and availability of active diagnostic ingedients (ADIs) in regions with endemic or neglected disease, a reverse transcriptase (RT) fusion construct is reported (Δ3R5-TGP-RT), having the same modular architecture (R5-fluorescent protein-functional enzyme) as reported previously by us. In tandem with the R5-mCherry-Bst this RT construct completes the enzyme set required for RT-LAMP mediated detection of Dengue. The introduction of the thermophilic green fluorescence protein TGP, allowed a heat purification step at 95 °C to be introduced into the workflow, simplifying purification. A 3 terminal amino acid (SSK) truncation of the naturally occurring silaffin R5 binding peptide (Δ3R5) enabled improved protein purification and loading on silica and good storage stabilisation (≥3 months). L-arginine triggered elution of enzyme from silica, immediately prior to use, enabled a soluble enzyme to be delivered directly into the RT-LAMP reactions, producing a clear solution and compatibility with turbidity detection of PPi released complexes that form insoluble $Mg_2P_2O_7$. A unique primer set was designed for the detection of Dengue Serotype 1 RNA, using a primer set (CAB 3), targeting the RNA-dependent RNA polymerase (RdRp), part of the NS5 region. This was chosen to minimise primer dimer formation, thereby reducing false positives. Amplification was achieved with high sensitivity (10 copies), with turbidity analysis able to distinguish positive and negative reactions. The approach developed has the potential to widen the application of LAMP diagnostics for neglected diseases such as Dengue by removing the availability of biological reagents as a limiting factor.

Introduction

Dengue fever is one of 20 neglected tropical diseases (NTDs) recognised by the World Health Organisation,[1] most severely affecting impoverished communities, with devastating health, social, and economic effects.[2] Dengue virus (DENV) is an arbovirus spread by bites of female *Aedes aegypti* and *Aedes albopictus* mosquitos.[3] It is currently the most rapidly growing and prevalent arboviral infection worldwide, surpassing both Zika and Chikungunya.[4] According to the Centres for Disease Control and Prevention (CDC), over half the world's population live at risk from DENV infection. The WHO estimate 100 million DENV infections per year across 127 countries, with 20 000 deaths resulting from infection.[5] Deaths are most likely to be recorded in endemic regions where more than one DENV serotype is present.[6]

aChemical Engineering and Biotechnology, University of Cambridge, Phillippa Fawcett Drive, Cambridge CB3 0AZ, UK. E-mail: eah16@cam.ac.uk

bResearch Center for the Natural and Applied Sciences, University of Santo Tomas, España Blvd., Manila, Philippines

† Current address: Institute for Manufacturing, University of Cambridge Alan Reece Building, 17 Charles Babbage Rd, Cambridge, CB3 0FS.
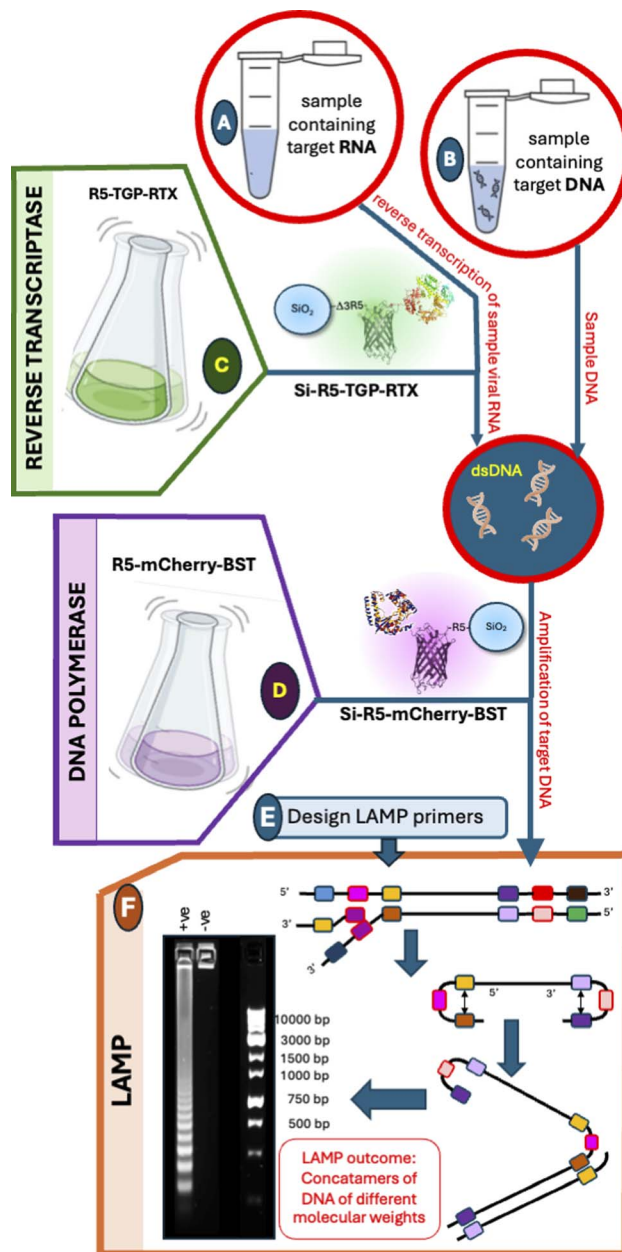
Dengue virus RNA can be detected with a nucleic acid amplification test (NAAT) in blood, serum, and plasma. Most of these tests identify the infecting dengue virus serotype. There are 4 primary serotypes within the DENV flavivirus family, which comprise the aetiological agent.[7] DENV infection may be asymptomatic but may also be characterised by life-threatening manifestations.[8] Severe DENV illness is associated with thrombocytopenia, plasma leakage, shock, bleeding and multiple organ failure.[9] These conditions occur mainly in children under 15 but are also associated with secondary infection with a new DENV serotype.[10] As DENV infection symptoms may vary and can mimic the manifestations of infections related to other aetiologic organisms, it is quite difficult to make an accurate clinical diagnosis.[11] Hence, it is necessary to utilise laboratory tests to have a definitive diagnosis. Whilst DENV nonstructural antigen1 (NS1) is widely used for detecting dengue, it has a low sensitivity (49 to 59%)[12] and cross-reactive antigens and antibodies have been documented for flaviviruses, *i.e.* dengue, West Nile, zika and Japanese encephalitis.[13] For this purpose, nucleic acid diagnostics which can either be targeted to triage DENV as the infecting species or can discriminate between individual DENV serotypes are of clinical interest.[10]

While NAAT for DENV has been developed,[14,15] access to the tests or even the active diagnostic ingredients (ADIs) for the tests are often limited in low-and-middle-income countries (LMICs), due to costs and supply chains. Up to 80% of the cost of a diagnostic test kit can be attributed to the enzymes utilised[16] which must be procured internationally, the consequences of which were highlighted during the COVID-19 pandemic, where supply chains to many LMICs were narrowed or removed completely.[17] DENV diagnostics remain unavailable in many under-resourced laboratories,[18] especially in rural health settings,[19] but diagnostics are essential for accurate patient management, disease surveillance and early identification of outbreak and control measures.

This study describes pre-clinical developments for a DENV RT-LAMP test designed to enable local production in the Philippines, without specialist protein production facilities. Dengue has been recorded in the Philippines for over a century, where it is endemic, and with the number of cases increasing, exceeding 200 000 p.a. since 2015. Recent studies have suggested some prevalence of all 4 serotypes across the 3 main island groups with low diversity.[20] However, DENV-1 is much more generally widespread than the other rarer serotypes and was the most prevalent recorded in 2023 (93% of cases). It has also shown persistence in endemic outbreaks and of a single genotype since 1974, whereas serotype 4, for example, has been associated only with more sporadic cases[7] The aim of this study was therefore, to produce the active diagnostic ingredients locally in the Philippines at low cost, primarily for a DENV-1 NAAT, without dependency on international supply chains.

This builds on previous work focused on developing a Bst polymerase for Loop-mediated isothermal amplification (LAMP) in malaria diagnosis, which was able to be produced at the testing-site in Ghana.[21] Core to the existing protein design is a polymerase fusion protein with recombinantly attached mCherry fluorescent protein, facilitating easy colorimetric calibration and quality control. The 'mCherry-Bst' was also fused with an R5 peptide-silaffin binding tag, providing an easy purification protocol and good stability of the immobilised enzyme, while enabling it to be utilised in the LAMP reaction in an immobilised state, on silica particles.

However, to provide a NAAT protein reagent production workflow for Dengue diagnostics, the sample is RNA rather than DNA (Scheme 1). Therefore, as the first step to enable RNA (virus) diagnostics to be linked with DNA amplification (Scheme 1 path A to F), creation of a reverse transcriptase (RT – Scheme 1C) with similar architecture to the field-successful Bst construct is investigated and a LAMP primer set (Scheme 1E) designed. The latter is needed to overcome the potential unsuitability of the normally favoured 3′UTR (untranslated region) target primer region, due to the presence of strong secondary structures, which typically result in a higher incidence of false positives. Design and laboratory testing of a reverse transcriptase construct is reported in this study and, the option to combine the benefits of silica immobilisation for enzyme isolation and storage stability is considered, integrated with enabling soluble eluted enzymes to be used for RNA reverse-transcription and DNA amplification.

Scheme 1 (A) RNA and (B) DNA pathways to (F) LAMP. Path (A) requires (C) RT and (D) Bst. Path (B) required only (D) Bst. Effective targeted LAMP (low false positives and false negatives) also requires good design of (E) the LAMP primers.

Materials and methods

Materials Q5 high fidelity polymerase master mix, NEB Turbo Competent *E. coli* (high efficiency), Bst 2.0 polymerase, magnesium sulphate (MgSO$_4$) solution, deoxynucleotides solution mix, nuclease free water, 10X isothermal amplification buffer, ThermoPol 10X buffer, RTx Reverse Transcriptase (the NEB commercially available RT), DNase I (RNase-free), 6X DNA loading dye, 1Kb Plus QuickLoad DNA ladder, 1Kb QuickLoad DNA ladder, 100bp DNA ladder, Monarch Plasmid Miniprep Kit, Monarch DNA Gel Extraction Kit, Monarch RNA clean-up kit, HiScribe® T7 high yield RNA synthesis kit, and NEBuilder HiFi

DNA assembly master mix were obtained from New England Biolabs. Silica gel 60 (<63 μm) was obtained from Fluka. SYBR™ Safe DNA gel stain was obtained from APExBIO. Pierce™ unstained protein MW marker was obtained from Thermo-Fisher Scientific. Ultrapure™ Agarose, NuPAGE MES SDS running buffer 20X, and NuPAGE 4–12% bis–tris 1 mm mini protein gels were obtained from Invitrogen™. Ni-NTA His-Bind® Resins were obtained from Novagen. LB agar, LB broth, kanamycin, TRIS acetate EDTA (TAE) 50X solution, and iso-propyl β-D-1-thiogalactopyranoside (IPTG) were obtained from Melford Laboratories. Lysozyme from chicken egg white, sodium chloride (NaCl), potassium chloride (KCl), sodium hydroxide (NaOH), hydrochloric acid (HCl), Triton-X-100, tris(hydroxymethyl)aminomethane (tris), sodium dodecyl sulphate (SDS), bromophenol blue, β-mercaptoethanol, di-thiothreitol (DTT), ethylenediaminetetraacetic acid (EDTA), ammonium sulphate ($(NH_4)_2SO_4$), and magnesium sulphate ($MgSO_4$) were obtained from Sigma Aldrich. BL21(DE3) competent cells were obtained from Agilent Technologies. 0.2 μm sterile filters were obtained from Sartorius. 50 000 NMWL Amicon® Pro regenerated cellulose centrifugal filters, and DNA primers were ordered from Merck. CentriPure 25-Z25M Zetadex Gel Filtration columns were obtained from emp BIOTECH. Quick Coomassie Blue Stain was obtained from Generon.

Assembly of (R5)n-mCherry-His10-Bst and TGP-RT

Assemblies used the plasmid backbone previously developed.[21] For TGP-RT a 2-step assembly was used, starting with the mCherry-BST construct and replacing mCherry with the TGP sequence, then Bst with RTX. PCR used Q5 2X high fidelity master mix, followed by gel extraction and assembly using NEBuilder. Assemblies were transformed into NEB Turbo cells. Constructs were verified using Genewiz sanger sequencing services. The correct plasmid was transformed into competent BL21(DE3) cells (Agilent), which were stored at −80 °C in 25% glycerol.

Expression of pET24a (+) fusion constructs in BL21(DE3)

Overnight cultures were grown at 37 °C, 225 rpm with 50 μg mL^{-1} kanamycin. Overnights were transferred to 200 mL LB with 50 μg mL^{-1} kanamycin until OD600 0.6–0.8, before induction with 1 mM IPTG. Bst constructs were expressed for 4–5 h at 37 °C. The TGP-RT construct, unless otherwise stated, was expressed at 18 °C for 18 h. After expression, 200 mL culture was transferred to 4 × 50 mL centrifuge tubes and spun for 30 min, 3000 rpm.

To optimise expression for TGP-RT, fluorescence was measured pre and post lysis using a Tecan Infinite® M200 PRO plate reader, ex: 493 nm, em: 507 nm (note this is a different instrument to that used for fluorescence calibration). Expression yields were studied at 37 °C for 4 h, 30 °C for 8 h, 25 °C for 12 h, and 18 °C for 18 h.

Heat purification of fusion constructs

Expressed pellets were thawed on ice and resuspended in 5 mL PBS with 1 mg mL^{-1} lysozyme. Suspensions were sonicated for 48 cycles, 1 s on and 4 s off, at a frequency of 35 kHz. For the TGP-RT, the sonications were heated to 95 °C (5 min), whilst gently mixing to prevent co-aggregation of the TGP-RT with mesophilic host protein, to enhance the protein solubility and purity. For the mCherry-Bst this step was included but performed at a lower temperature of 65 °C. Suspensions were centrifuged at 4800 rpm for 30 min. Cell lysate was syringe filtered (0.2 μm).

Silica purification of fusion constructs

The silica purification methodology followed previous studies.[21] Storage buffers were as follows: mCherry-Bst: 2.5 mM tris–HCl, 30 mM KCl, 1 mM DTT, 25 μM EDTA, 0.1% Triton X-100, pH 7.2. TGP-RT: PBS at pH 7.4–137 mM NaCl, 2.7 mM KCl, 2 mM KH_2PO_4, 10 mM Na_2HPO_4. For $(R5)_n$-mCherry-Bst immobilisation study, the lysate and supernatant (after immobilisation) fluorescence were measured using a Tecan Infinite® M200 PRO plate reader, ex: 587 nm, em: 610 nm (blanking with PBS). 0.5 mL lysate was added to 10 mg silica for this experiment only, whereas 20 mg silica (1 mL lysate) is used as standard. For the mCherry-Bst and TGP-RT saturation study, fluorescence was measured pre and post immobilisation and calibrated to mass via the fluorescence calibration methodology.

Fluorescence calibration

His purified enzyme was used to minimise contaminating proteins, ensuring direct reporting of fluorescence units to the enzyme. Enzymes were diluted in triplicate, with the concentration and fluorescence measured at each dilution. Concentration was measured using a Nanodrop™ spectrophotometer, using custom extinction coefficients and molecular weights; TGP-RT: MW = 119.242 kDa, ε = 155 400 M^{-1} cm^{-1}; mCherry-Bst: MW = 96.591 kDa, ε = 90 190 M^{-1} cm^{-1}. Fluorescence (mCherry or TGP) was measured using a BMG LabTech FLUOstar Omega plate reader. Calibrations and corresponding SDS-PAGE can be found in SI (Section S1 Fig. S1). The fluorescent calibration curves estimated using the mCherry and TGP tags (SI, Fig. S1) were used to control mCherry-Bst and TGP-RT enzyme units through assay optimisation, facilitating normalisation between batches.

SDS-PAGE protein analysis

Protein samples for SDS-PAGE analysis were prepared by adding; 1 μL protein sample, 9 μL water, 5 μL 3X loading dye (1X loading dye: 62.5 mM tris–HCl pH 6.8, 2.5% SDS, 0.002% bromophenol blue, 0.7135 M β-mercaptoethanol, 10% glycerol). The Invitrogen NuPAGE® Novex® Gel System was used (175 volts for 50 min, MES buffer). Gels were stained overnight in Quick Coomassie before de-staining in water for 48 h.

Preparation of dengue target DNA and RNA

Dengue serotype 1 DNA (accession number NC_001477.1, position 6377 to 10 735) was ordered from Twist Bioscience, as a clonal plasmid. The fragment incorporates the non-structural protein NS4A, non-structural protein NS4B, RNA-dependent RNA polymerase (RdRp) NS5, and 3′ UTR. The plasmid was

transformed into NEB Turbo cells and colonies grown overnight (LB, 50 μg mL^{-1} kanamycin, 37 °C, 225 rpm). Overnight colonies were miniprepped and plasmid concentration determined using a NanoDrop ND-1000 Spectrophotometer. The RdRp gene was amplified using a forward primer containing a 5′ T7 promoter for later transcription, using Q5 master mix. Products were gel extracted and quantified. A dilution was performed using nuclease free water to yield a 10^8 copies per μL stock solution. The initial fragment (prior to dilution) was used for transcription (T7 HiScribe Kit) to generate RNA, including a DNase I digestion and Monarch RNA Purification Kit steps. The RNA was quantified and serial dilutions performed to yield stock solutions of 100 k, 10 k, 1 k, 100, and 10 copies per μL.

RT-LAMP LOD assays

Primer sequences for the CAB3 set are in Table 1. 25 μL RT-LAMP reactions consisted of 1X isothermal amplification buffer (NEB), 1.4 mM each dNTP, 6 mM MgSO$_4$, 1.6 μM of FIP and BIP, 0.2 μM of F3 and B3, 0.4 μM of LPF and LPB, 1 μL of RNA stock at desired copy number/μL, relevant polymerases, and made up to 25 μL with nuclease free water. For reactions containing NEB Bst 2.0, 1 μL enzyme was used (8 units); for those with NEB RTx, 0.5 μL was used (7.5 units). Eluted mCherry-Bst or TGP-RT were diluted to facilitate 1 μL enzyme addition post-elution. The reactions were heated to 65 °C for 30 min (in Eppendorf Mastercycler). Turbidity was measured post-reaction at 750 nm (BMG LabTech FLUOstar Omega plate reader).

RT-LAMP testing for DENV-1 in Manila

CAB2, CAB3, and CAB5 sets were first screened using synthetic DNA and commercial Bst 2.0, following the described LAMP methodology for 60 min (CAB2 and CAB5 sequences are given in S2, Table S1). LAMP primers were designed using NEB® LAMP Primer Design Tool (New England Biolabs). The RdRp gene (NCBI Reference: NC_001477.1) was grouped into two queries (nucleotides 1–1000 and 693–1692) to ensure full gene coverage. The outputs (comprising of 4 primers – F3, B3, FIP and BIP) were first screened for compatibility with a 6 primer LAMP configuration (suitable spacing between the F1–F2 regions and B1–B2 regions). For every viable set, LF and LB primers were designed to be between 18–24 nucleotides long and with a comparable Tm to the F3/B3 primers of that set, while meeting a minimum threshold of 50 °C. Lastly, the primer sets were screened for non-specific annealing potential using Oligo

Analyser 1.0.2. Any spontaneous (negative ΔG) self-hybridisation or primer-dimerisation was recorded for every primer within a set and the overall potential was normalised by summing all free energy values for every spontaneous self-hybrid and primer-dimer configurations of a specific primer and dividing the total with the free energy for that primer to bind to its complementary sequence.

Arginine elution of silica-immobilised constructs

The sample was centrifuged at 7000 rpm for 5 min and the storage buffer removed. For a 20 mg sample, 50 μL of 0.5 M L-arginine was added and the sample resuspended and incubated at room temperature for 10 min, vortexing halfway. The suspension was spun at 7000 rpm for 5 min and the supernatant (eluted enzyme) removed and diluted 1 : 2 in the relevant storage buffer to yield 100 μL eluted construct. For arginine elution characterisation, dilutions of L-arginine from 1 M were made and added as per standard elution protocol but were linearly scaled to 10 mg silica. Eluted enzyme mass was determined using fluorescence calibration.

Results and discussion

Optimising the R5 silaffin peptide immobilisation tag in mCherry-BST

We have previously reported on *de novo* set-up and local production of an engineered Bst polymerase fusion protein (mCherry-Bst-see generic architecture later). This was used in NAAT for malaria diagnosis in Ghana *via* LAMP,[21] where the target is a DNA malaria template (Scheme 1 entry point B). It has also been trialled during Covid19 (ref. 22) (together with a commercially available reverse transcriptase) and in other infectious disease scenarios (*e. g.* Cholera, Leptospirosis *etc*). One of the features of the BST fusion protein used in trials showing DNA amplification (Scheme 1 starting from point B), was its self-assembly on silica *via* an R5 silaffin peptide tag, thereby avoiding the need for expensive His-tag-purification (or other cost prohibitive materials for downstream processing) in the standard operating procedure, for enzyme production. Bst can be used in LAMP still attached to the silica. This is advantageous because it stabilises the protein during storage, enabling a longer shelf-life with less dependency on cold-chain facilities.

The R5 peptide is therefore a design asset and taking further inspiration from other silica affinity peptides such as Car9 where a 3K (3 × lysine) content motif is found, the wildtype R5

Table 1 CAB3 LAMP primer sequences

CAB3 primer	Sequence (5′ to 3′)
F3	CAATATGGTACATGTGGTTGG
B3	GGCTGTGTCATCTGCATAC
FIP	ATTCTCTCTGCTGAACCAGTGATCCGCGCTTTTTAGAGTTTGA
BIP	TCACTCAGTGGAGTGGAAGGAATTTCCCCCTGGAATCTTTG
LF	TCATTCATGAAACCAAGGGC
LB	ACTTGGATACATACTCAGAGAC

tag (SSKKSGSYSGSKGSKRRIL) used thus far, was truncated by 3 terminal amino acids-SSK (named Δ3R5), to establish whether higher silica immobilisation efficiencies and even better performance could be achieved for the mCherry-Bst with this shortened motif. The electrostatic interactions between basic K and R residues present in R5/Δ3R5 drive association with the negatively charged silica surface.[23] As such, a reduction in basicity may seem counterproductive to enhance binding affinity. However, it has been reported that removal of the N-terminal serine residues correlates with the biomineralisation of smoother silica particles, which could be associated with more compact packing.[23]

In this context, the number of R5 units was also investigated to establish a trend between binding efficiency and R5 content in comparison with a single Δ3R5. A negative correlation between total R5 content (repeat motifs) and binding efficiency was observed (Fig. 1A) which may correlate with different packing efficiency within and between the tags, influencing association with neighbouring proteins as well as between protein and the silica. Although, bigger (negative) differences are found by increasing the number of R5 repeats, the 3-residue-deletion 'Δ3R5' sequence demonstrates greater binding affinity for the mCherry-Bst tagged protein (increasing from $87 \pm 0.5\%$ to $93 \pm 0.4\%$ immobilisation efficiency when tested with 10 mg silica and ~0.5 mg mL^{-1} enzyme). Also, due to the consistency of improvement with the 'Δ3R5', the result showed a statistically significant improvement (two-tailed $p = 0.0016$), so the modified Δ3R5 was incorporated into the generic construct template.

Recombinant RT protein design

The polymerase alone does not give access to viral RNA targets, without reverse transcriptase activity to convert the RNA into DNA. Adopting the same recombinant architecture approach, a reverse transcriptase fusion enzyme was designed with equivalent functional modules (Scheme 1 starting from point A, Fig. 2A and 3A), namely: the R5/Δ3R5 silica binding tag at the N-terminus; fluorescent protein for visualisation, calibration and quality control; and the functional RT at the C-terminal region. Modules were separated by flexible linker regions (GGGSG) to promote correct folding of the recombinant components.

The Ellington group's RTX,[24,25] is derived from KOD polymerase by directed evolution (it is not to be confused with RTx, a commercial RT from NEB). It exhibits bifunctionality, retaining the parental PCR activity in addition to the engineered RT capability. Like KOD polymerase, high thermostability is observed in RTX, compatible with PCR denaturation temperatures (95 °C), so that it is expected to show appropriate thermostability and activity for LAMP (minimum requirement 65 °C).

In Fig. 2A the common recombinant architecture, highlights the interchangeable units for the Bst and RT, but, additionally in the case of RT, the mCherry calibration-tag was replaced with thermostable green protein[26] ('TGP-RT' see Fig. 3A). This provides two advantages: using a different fluorescent protein for the RT, enables clear distinction in calibration of RT/Bst (see cartoon in Scheme 1), whereas its stability up to 95 °C
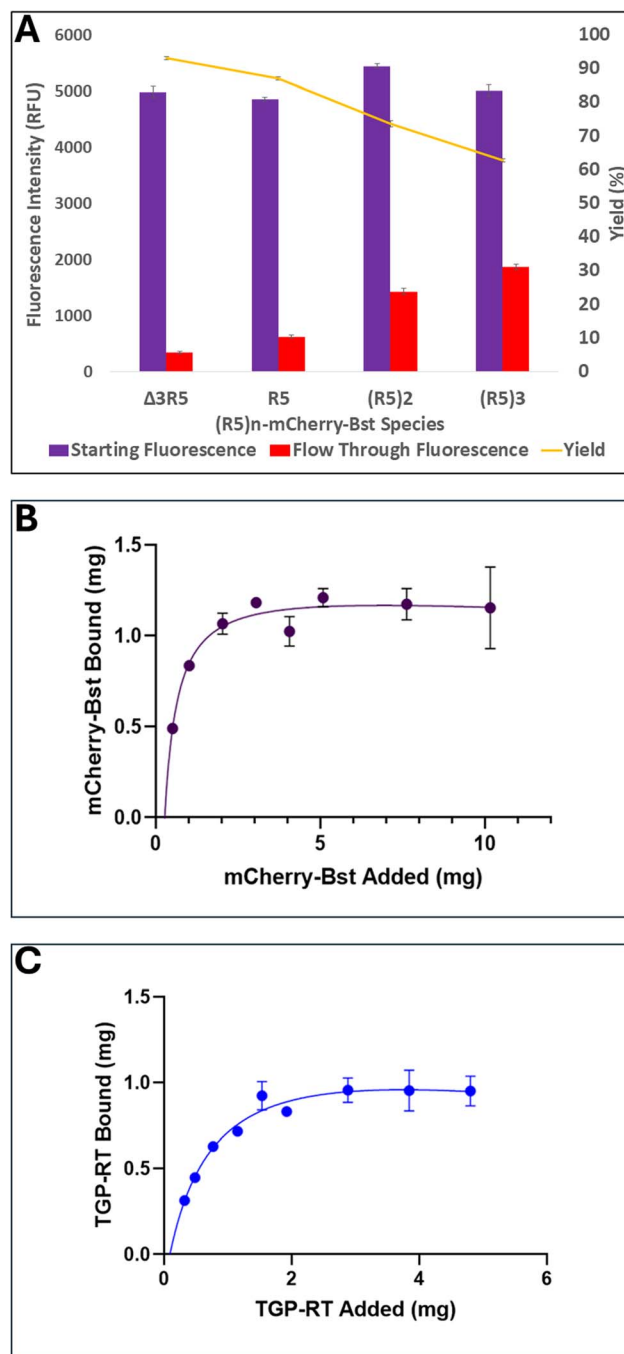

Fig. 1 (A) Binding efficiency of different mCherry-Bst recombinants, with modified (Δ3R5) or increasing R5 units, measured by relative fluorescence loss (mCherry ex: 587 nm, em: 610 nm). 0.5 mg mL^{-1} protein was assayed with 10 mg 60 μm silica particles. (B) Δ3R5-mCherry-Bst silica binding isotherm, yielding $B_{max} = 1.170$ mg/20 mg silica, with R2 value 0.9473. (C) Δ3R5-TGP-RT silica binding isotherm, yielding $B_{max} = 0.985$ mg/20 mg silica, with R2 value 0.9728. Data was fitted to a one site binding curve using Prism software, $y = (B_{max} \times$ [added protein])/(K_d + [added protein]), where B_{max} is the maximum bound protein.

introduces the possibility that heat-denaturation can be used to destroy the mesophilic host (*E. Coli*) proteins in the cell lysate while retaining the desired thermostable TGP-RT protein
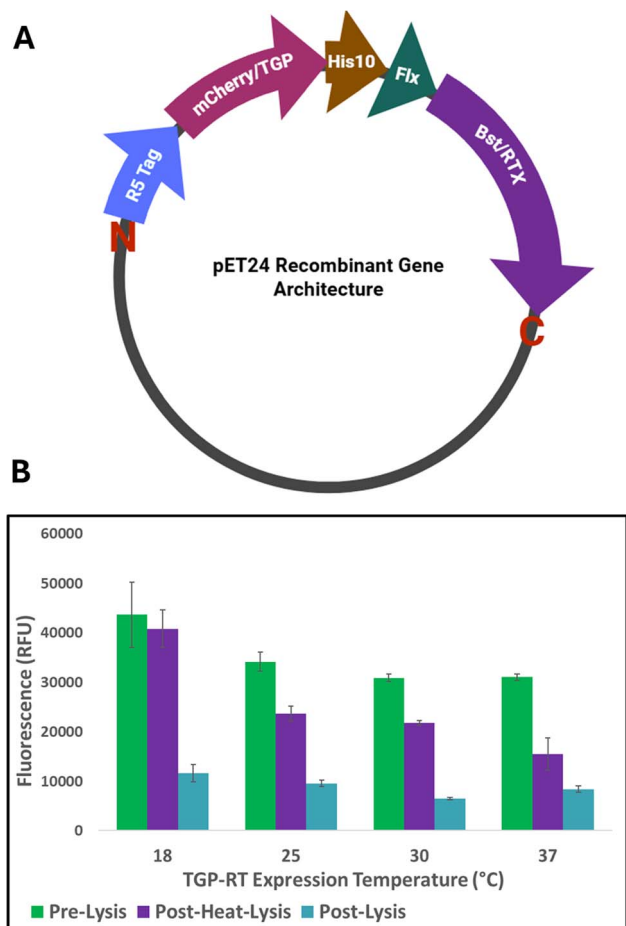
Fig. 2 (A) Generic pET24a(+) architecture, produced using BioRender™. Protein N and C terminals are indicated; 'Flx' refers to a flexible linker region-GGGSG. (B) Relative fluorescence values (TGP ex: 493 nm, em: 507 nm) after expression of TGP-RT (pre-lysis) and after lysis with and without heat-purification, at different expression temperatures, with SEM bars shown.

construct. This would achieve "heat-purification" without any formal chromatographic methodology (Fig. 2B). This underused technique (especially suitable in LMICs) imparts a significant advantage for the RTX over other less thermostable RT's (MMLV and AMV mutants).

In the case of this RT construct, a lower expression temperature (18 °C) correlates with higher yield, with exceptional net yields of TGP-RT after cell lysis, only when the 95 °C heat-step was incorporated. Over 90% yield (compared with pre-lysis) could be obtained from a culture expressing at 18 °C when heat-purification was used. Without heat-step incorporation, yields were low. Although the heat-step appears able to partially resolubilise TGP-RT aggregates, the effectiveness of this is also reduced at higher expression temperatures. The observed correlation between expression temperature and yield correlates with greater TGP-RT inclusion body formation at higher temperatures.

Initial testing of the heat purified TGP-RT lysate for upstream RNA transcription in a RT-PCR reaction to amplify 675 and 240 bp amplicons showed good activity (Fig. 3b), suggesting that the TGP-RT was functioning as required.
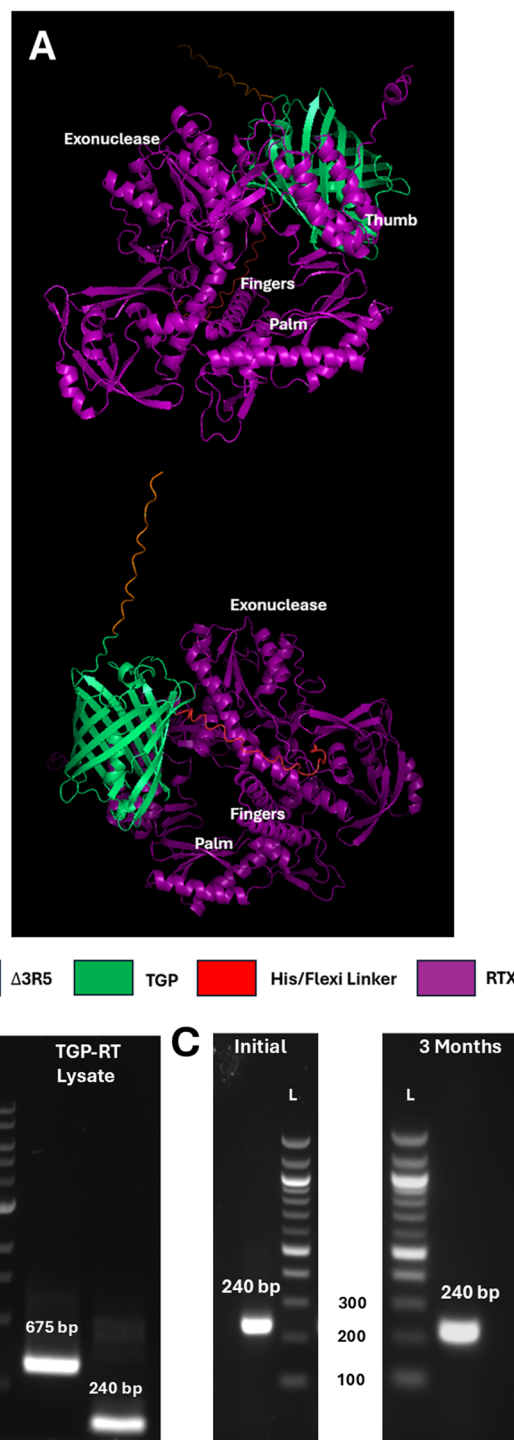

Fig. 3 (A) Modelling of TGP-RT using alphafold 3 and PyMol, with polymerase domains labelled. In the second image, the thumb domain is obscured by TGP (see also Fig. S2 with Alphafold confidence scores) (B) PCR reactions using heat-purified TGP-RT lysate, to amplify a 675 and 240 bp amplicon. (C) PCR using immobilised TGP-RT, initially and after 3 months storage at 4 °C.

Comparing silica immobilisation of TGP-RT and mCherry-BST

The mCherry-Bst construct[21] has demonstrated that silica immobilisation provides a low cost and robust protein purification and storage method, with the enzyme also able to be

utilised in an immobilised state.[16] Despite being a fusion protein, Fig. 3A predicts the individual character of the component proteins and peptides is retained in the new TGP-RT construct and the Δ3R5 component does not become buried into the protein, but remains protruding and available for interaction with a silica particle. Furthermore, as for mCherry-BST, a similar enhanced stability was demonstrated by the TGP-RT, when immobilised on silica, with undiminished activity after 3 months of storage at 4 °C (Fig. 3C).
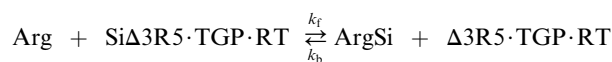
A slightly lower immobilisation coverage was obtained for the TGP-RT (0.989 mg per 20 mg silica) compared with the mCherry-Bst (1.151 mg per 20 mg silica), with half saturation loading of the same order – 0.471 and 0.593 mg respectively. Modelling the surface charge at pH 7.4 for TGP, mCherry, Bst,
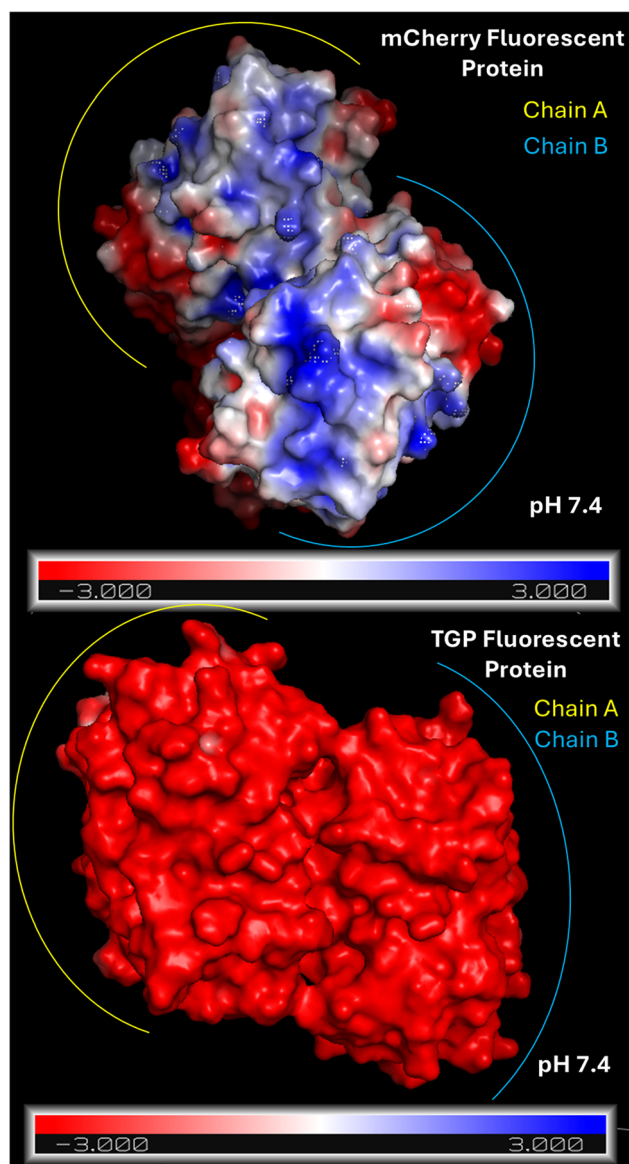

Fig. 4 Surface charge models of mCherry (PDB: 4ZIN) and TGP (PDB: 8TJH) fluorescent proteins prepared with PDBQ2PR/APBS software and visualised using PyMol. Chains A/B represent repeat units present in crystal structures. Proteins were modelled at pH 7.4, analogous to pre-elution pH. Scale showing −3 to +3 kT e^{-1}.

and using KOD polymerase from PDB structures as the model for RTX (from which it is derived[24,25]), shows stark contrasts between mCherry and TGP (Fig. 4). Whilst the TGP is highly acidic, and does not appear capable of strong associations with negatively charged silica particles, the mCherry has significant regions of positive potential. Due to the beta-barrel structure of the protein, these regions are highly accessible and likely result in extended interactions between mCherry and silica, which may account for the slightly higher silica loading with this construct. Hellner *et al.*[28] have proposed that in their immobilisation of mCherry and sfGFP to silica *via* the Car9 silaffin peptide, the surface of mCherry from which the Car9 is attached has a higher electrostatic potential than for sfGFP, which might minimize short-range electrostatic interactions between the mCherry and the silica, allowing Car9 to more efficiently interact with the silica surface. A Green Fluorescent protein has also been engineered to tailor its electrostatic surface charge to allow direct oriented immobilisation on silica, without denaturing,[29] so it is reasonable to assume that while the affinity may be driven by the Δ3R5 association with the negative silica surface, there may be additional secondary interactions, particularly with the mCherry, influencing the immobilisation.

Elution of fusion constructs

Although, the enzyme will function while still on the silica, the presence of silica interferes with one of the simplest and lowest cost methods commonly utilised in LAMP product detection, namely turbidity. The DNA synthesis pathway in the Bst polymerisation is initiated by the association of the incoming dNTP in the active site, adding dNMP to the DNA strand synthesis, releasing pyrophosphate (PPi). The released PPi complexes with divalent ions such as Mg^{2+} to form insoluble $Mg_2P_2O_7$. Due to the large quantity of DNA produced by LAMP, the reaction induces a change in turbidity. However, silica prevents the implementation of a turbidimetry measurement (since the silica particles themselves scatter light).[27] Thus, in this instance, it would be advantageous to release the enzyme from the silica in a workflow upstream of the DNA amplification.

The electrostatic association between silica and basic K and R residues in the Δ3R5/R5 tags, suggests that this interaction could be disrupted. Since these constructs are not halophilic proteins, high salt concentrations (eg NaCl) would cause disruption of the hydration shell, increase hydrophobic interactions and protein aggregation and precipitation. However, by using a free basic amino acid, for example, ʟ-arginine, the enzyme could be eluted from the silica *via* a competitive binding process, which would be expected to displace the arginine and lysine side chains present within the Δ3R5 tag, according to the exchange with the silica bound TGP-RT (SiΔ3R5.TGP.RT), releasing the TGP-RT (Δ3R5.TGP.RT).

$$\text{Arg} + \text{Si}\Delta 3\text{R5}\cdot\text{TGP}\cdot\text{RT} \underset{k_b}{\overset{k_f}{\rightleftharpoons}} \text{ArgSi} + \Delta 3\text{R5}\cdot\text{TGP}\cdot\text{RT}$$

1

Arginine is known to act as a chaotrope, disrupting hydrophobic interactions causing aggregation and aiding in protein

refolding.[30,31] Together with arginine's derivatives these benefits depend on the net charge and concentration. Although not all the protein can be recovered during the arginine elution process, results in Fig. 5 suggest that L-arginine (R) can effectively displace the Δ3R5 tag from silica. From Fig. 5, ∼69% eluted TGP-RT (258 ± 5.5 μg) was achieved, at arginine concentrations ≥ 500 mM. However, for the mCherry-Bst, the yield was significantly smaller, with just 33% of enzyme recovered (133 ± 4.5 μg), even at high arginine concentration.

Taking the basic exchange equilibrium described in eqn (1), and considering just the exchange of L-arginine with the Δ3R5-immobilised Bst or RT construct at the silica surface, allows a comparison of L-arginine induced elution according to:

$$\frac{[\text{ArgSi}][\Delta 3R5 \cdot \text{TGP} \cdot \text{RT}]_{\text{sol}}}{[\text{Si}\Delta 3R5 \cdot \text{TGP} \cdot \text{RT}]} = K_{\text{eq}}[\text{Arg}]_{\text{sol}} \quad (2)$$

This is plotted in Fig. 5C, from which the extent to which the reaction proceeds, displacing the protein from silica in the presence of L-arginine, is nearly an order of magnitude greater for the TGP-RT than the mCherry-Bst. Furthermore, it can be seen from the figure that a threshold concentration of arginine is required, so that elution of the mCherry-Bst is not significant below 100 mM, giving an apparent K_{eq} of 8×10^{-5} (low

concentration non-elution offset 60 mM). In contrast at 100 mM L-arginine ∼30% of the TGP-RT has been eluted which has an apparent K_{eq} of 5×10^{-4} (offset 10 mM). Given the similarity in the immobilisation curves and good fit to a simple one site binding/elution isotherm, this appears to reinforce the discussion above, that for mCherry other interactions are occurring between the silica and the mCherry, that are not disrupted easily by the L-arginine. Electrostatic and hydrophobic interactions between the family of fluorescent proteins and silica have been widely reported, and differ between different members of the fluorescent protein family, as discussed above, based on the surface charges (Fig. 4). Therefore, depending on the overall organisation of the silica immobilised construct at the surface, the competitive displacement by L-arginine of both constructs may be constrained by more than just the Δ3R5 affinity peptide. At the alkaline pH anticipated with L-arginine (pK_{a} 12.5) at sufficiently high concentration, the modelling showed highly negative surface charges dominating all the proteins in these constructs (SI Fig. S3–S5). However, this doesn't take into account that the surface interactions with the mCherry are formed during adsorption to silica, and they too must then be disrupted during elution. These may also reduce the extent to which L-arginine can access and compete, or rather deprotonate exposed protein side chains, thereby reducing elution efficiency.

Despite the differences in the elution efficiency, since the apparent activity of the eluted soluble enzyme is higher than the immobilised enzyme, less enzyme is required for the NAAT, leading to no overall reduction in test capacity per culture-batch. This elution-at-point-of-use method allows the benefits of storage of the enzyme on silica to be retained, with elution directly into the test system. The eluted proteins appear to be of good purity, comparable with the use of Ni-His chromatography. Band patterns (Fig. 5) around the target size are consistent with patterns observed with His-purified enzymes used for fluorescence calibration (SI – Fig. S1) and additional bands are thought to result from fluorescent protein breakdown on the gel.[32]
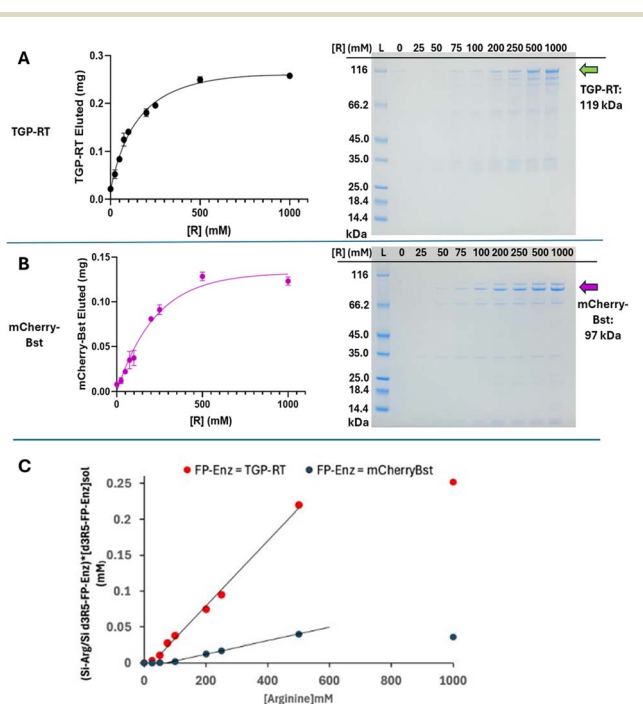

Fig. 5 (A) Si-immobilised protein elution model from 10 mg silica, utilising different L-arginine concentrations, modelled as elution from a PrismTM one site binding curve, $y = (B_{\text{max}} \times [\text{protein eluted}])/(K_{\text{d}} + [\text{protein eluted}])$, where B_{max} is the maximum eluted protein. (A) TGP-RT (with 0.375 mg TGP-RT bound prior to elution) yielding a maximum value of 0.258 mg enzyme ($R^2 = 0.9885$). (B) mCherry-Bst with 0.400 mg bound prior to elution, yielding a maximum value of 0.133 mg enzyme ($R^2 = 0.9692$). SDS–PAGE gel of the eluted samples are shown for A and B. (C) Plot derived from eqn (2) comparing K_{eq} for silica immobilised TGP-RT and mCherry-Bst from the slope of the curve (Data taken from averages obtained in A and B).

Design of LAMP primer sets for Dengue serotype 1

Before being able to test the mCherry-BST + TGP-RT combination for Dengue diagnostics (Scheme 1 starting from point A), a LAMP primer set needed to be designed (Scheme 1E). As described earlier, DENV-1 was selected for targeting, as it is endemic to the Philippines, has recently been the most detected serotype (>90% in 2023),[20] and has low genotypic shift, enabling ease of selectivity during screening. Currently, other serotypes have too low incidence, so would be less cost-effective testing targets in routine triaging to determine treatment pathways that distinguish, say, Leptospirosis and Dengue and thereby determine antibiotic use. The dengue virus (DENV) is a member of the *Flaviviridae* family with a positive-sense single stranded RNA genome. When selecting a target region for DNA amplification and subsequent diagnosis, it is considered advantageous to focus on the 3′-end of the genome. This is due to the 3′-end being the initiation site for genome replication and thus

selectively pressured to contain mechanisms for 3′-end protection.[33] This reasoning may explain the choice of the highly conserved 3′ UTR (untranslated region) between the 4 DENV serotypes, that has been greatly utilised by various RT-PCR systems.[34–36] However, due to the presence of strong secondary structures in the 3′UTR,[37] this region is unsuitable for LAMP

primers, as the primers (which would cover 8 regions over a 200–250 nucleotide section) would be partially complementary to each other, leading to a high likelihood of false positives. This may explain a widespread problem with many Dengue primers that have been extensively trialled and are available commercially, but give false positive rates.

In view of these issues, the RNA-dependent RNA polymerase (RdRp), part of the NS5 region, was chosen as a potentially better LAMP-diagnostic target here, due to its favourable location on the viral genome, and less unfavourable secondary structure (in comparison to the 3′UTR). Although this may perturb serotype specificity, the use of 6 primers during LAMP, can result in higher specificity than can be assumed in PCR.

Three primer set designs (CAB2, CAB3, and CAB5) (Fig. 6B and SI S2) were selected for investigation, and the commercial Bst 2.0 (NEB) was used first for their characterisation. The CAB3 primer set demonstrated the highest sensitivity during initial screening in the Philippines, with concatemer smears (characteristic of LAMP, Fig. 6A showing 2 repeats) even with just 10 copies of starting template. CAB2 did not exhibit false positive smears in the negative reactions (which would have been indicative of primer dimerisation) but the sensitivity was significantly lower than CAB3 (∼1000 copies). CAB5 produced unreliable sensitivity in addition to smearing in one of the negative reactions, ruling out selection of this primer set as a potential dimer-former. This emphasises the differences due to very small changes in primer positions (Fig. 6B). Although consideration is given at the primer design stage to eliminate sets prone to dimerisation (by evaluating free energies of potential dimers using OligoAnalyser™), dimers can still propagate. LAMP is particularly prone to such non-specific amplification because of the increased number of primers (6). By normalising the dimer free energies (both homo and hetero) against the free energy of full complementary binding (see eqn (3) below), the average resulting energies were found to correlate with the observed amplifications in Fig. 6A.

$$\frac{\sum_{\text{homo non-specific binding}} \Delta G + \sum_{\text{hetero non-specific binding}} \Delta G}{\Delta G_{\text{complementary binding}}}$$

3

Of the primer sets selected, CAB3 showed the best performance against DENV-1. This primer set exhibited the lowest average normalised free energy, as well as the lowest individual energies for FIP and BIP, which initiate strand invasion (Table 2). This presents a strong primer set candidate for point-of-need DENV-1 testing in endemic regions. In contrast, CAB5 displays the highest average and individual energies for FIP/BIP.

The prospect for the CAB3 primer set, to serve in distinguishing DENV-1 from the other serotypes can be assessed *in silico* through the hybridisation of complimentary regions to elucidate CAB3 specificity (Fig. 7). In addition, alignment of various DENV 1 isolates against the CAB3 binding region predicts high complementarity with the serotype 1 variant pool (SI Fig. S6).

Whilst complementarity was high for the F3 and B3c primers across serotypes 2–4 in the RdRp domains, it is the FIP and BIP
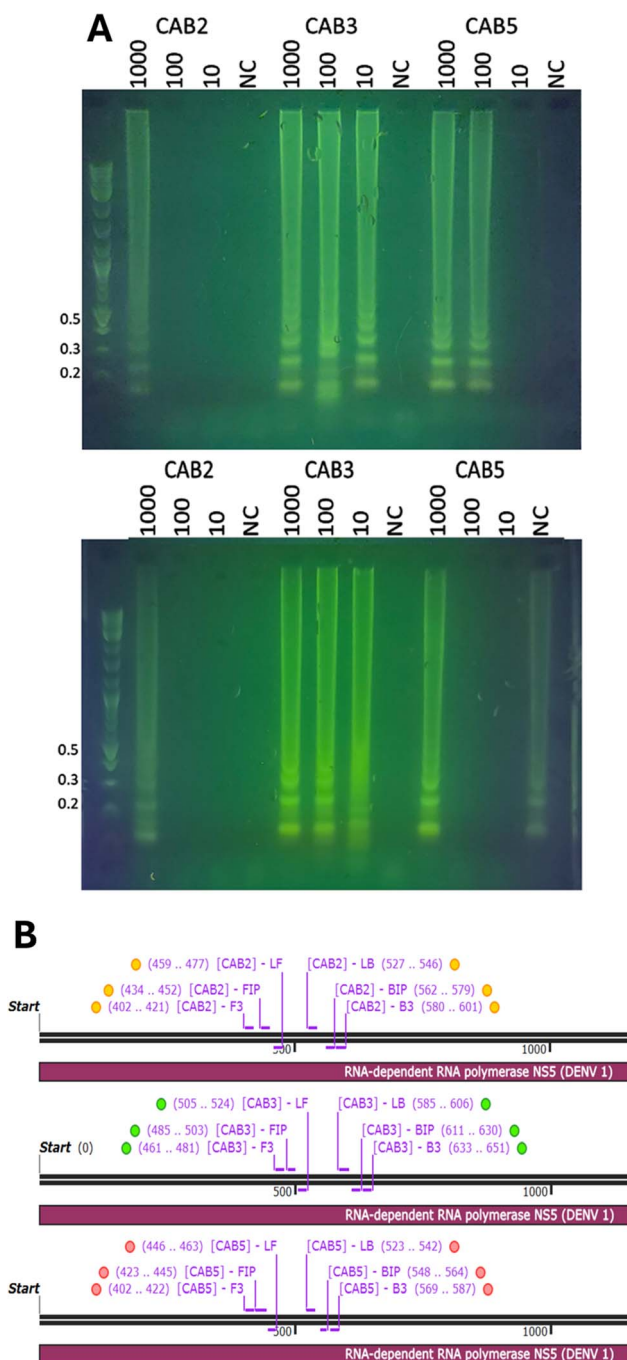

Fig. 6 (A) LAMP reaction screens of the CAB2, CAB3, and CAB5 primer sets using Bst 2.0 (NEB), in a 60-minute assay at UST Manila. 2 repeats are shown, with 1000, 100, 10, and 0 (marked NC-negative control) starting copies of synthetic DENV S1 RdRp DNA. NEB 1 kb plus DNA ladder was included with 0.2, 0.3, and 0.5 kb bands indicated. (B) Indication of primer set localisation to the RdRp NS5 DENV1 genome, for CAB2, CAB3, and CAB5.

Table 2 Normalised free energies (kcal mol^{-1}) of all dimer pairings (homo and hetero) against the free energy of full hybridisation, calculated using OligoAnalyser™

	F3	B3	FIP	BIP	LF	LB	Average
CAB2	1.32	0.85	1.38	1.52	1.29	0.67	1.17
CAB3	1.09	0.42	1.07	1.10	1.69	0.94	1.05
CAB5	1.41	1.59	1.31	1.33	1.60	1.15	1.40

primers which are responsible for strand invasion, and inherent formation of the LAMP starting dumbbell structure. Consequently, it is the FIP/BIP primers which mostly determine specificity. Since the equivalent B2 region (the 3′ end of the BIP primer which is complementary to the target) of the other serotypes show low complementarity to serotype 1, hybridisation at 65 °C should be strongly impeded for these serotypes, making observable amplification unlikely within the reaction timeframe for testing. Furthermore, although the B2 complementarity was slightly higher for serotype 3 (65%). This was coupled with a lower F2 (target sequence region in FIP) complementarity than with DENV 2 and 4, also pointing to good specificity for CAB3. Additionally, any hybridisation for the F3/B3 primers will possess a lower T_M, which will reduce hybridisation efficiency at 65 °C. Hence, it is concluded that the CAB3 set should show serotype specificity to DENV 1. As severe Dengue in some regions can be associated with secondary infection with a different DENV serotype,[10] this serotype-specific primer set could better aid clinical decision making.

CAB3 testing with silica-eluted enzymes

Using the CAB3 primer set targeting the RdRp (NS5) DENV S1 RNA sequence as described above, a limit of detection between 10–100 copies was obtained (Fig. 8A–C). However, the enzyme

Fig. 7 Clustal alignment of CAB3 and DENV serotype 1 (100% complementarity) – top rows, (NC_001477.1) against DENV serotypes 2–4 (OR501013.1, LC793497.1, OQ567872.1) – bottom rows, for the CAB3 primer binding regions indicated.

concentration is important for sensitivity, but also to avoid primer dimer formation. Thus, careful control and optimisation of the enzyme concentration was undertaken (facilitated by using the calibration via the mCherry and TGP tags; see Materials and methods) to maintain the mCherry-Bst concentration constant (2.5 µg), while adjusting the TGP-RT concentration. As see in Fig. 8A, where there are primers but no DENV template, the highest concentration of TGP-RT (5 µg per reaction) appears to produce a false positive outcome. At these high enzyme concentrations, less favourable reactions were also selected within the 30-minute reaction time, like primer dimer formation, despite poor complementarity, so the aim is to use the minimum required enzyme concentration to achieve a sufficiently sensitive result. In this case 2.5 µg per reaction was selected for both the mCherry-Bst and the TGP-RT.

Fig. 8B and C shows that the eluted enzymes performed similarly to the commercial alternatives, with consistent detection at 1000 copies. However, in both cases the amplification close to the LOD was variable. Thus, the silica eluted enzymes typically achieved 10 copy amplification in >50% of repeats. In contrast the commercial enzymes typically amplified down to 10 copies in only ∼30% of cases. The variability in these results is typical of NAAT outcomes utilising commercial NEB Bst 2.0 enzyme, with other studies and clinical trial data reporting inconsistent DENV 1 detection with primer sets targeting the commonly utilised 3′ UTR region[38] for samples with just 10 starting copies, only <40% reactions amplifying with synthetic template.

One ambition in eluting the enzyme from the silica, was to achieve a silica-free reaction solution where turbidity caused by the formation of the insoluble $Mg_2P_2O_7$ by product could be measured by absorbance (A750) (Fig. 8D). Typically, in previous LAMP trials, with a Bst attached to silica, the background turbidity was at least three orders of magnitude greater than the highest measurement obtained for 1000 starting copies in a silica free reaction. For the eluted enzyme LAMP reaction recorded here, the turbidity intensity correlated quite well with the image J digitalisation of the concatemer amplified DNA bands in Fig. 8C, taking into account that the image measurement is measuring intensity of separated and/or smeared DNA, whereas the turbidity measurement is related to the by-product of $Mg_2P_2O_7$ formation. Although the protocol and measurement system design needs optimisation for full integration with the LAMP and use in an LMIC, there was a statistically significant difference in the turbidity measurement between 0 and 10 copies across all repeats (two-tailed T-test, yielding a P value of 0.0012), whereas the electrophoresis/imaging results for the same experiment suggested the difference between 0 and 10 copies was not significant in all repeats. By quantifying the reaction outcome, this measurement could remove user experience from the interpretation of results, reducing ambiguity, although the repeatability of LAMP amplification close to its detection limit is always variable.

Overall, purification and storage of enzymes on silica, with subsequent L-arginine elution, demonstrates both desirable stability and activity, rivalling commercial alternatives without
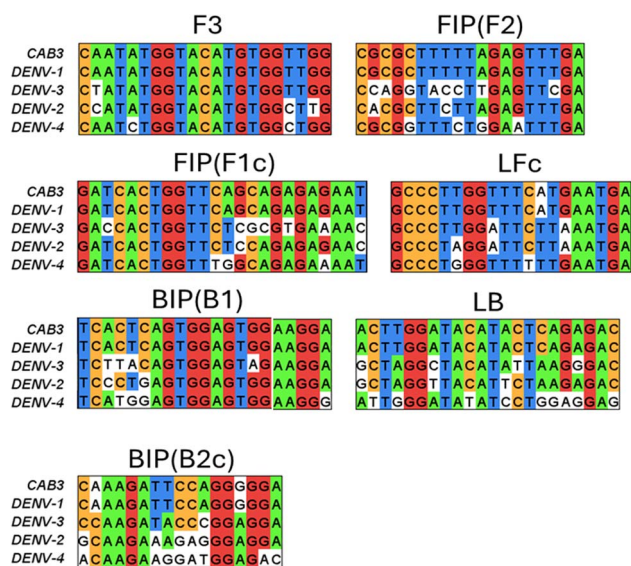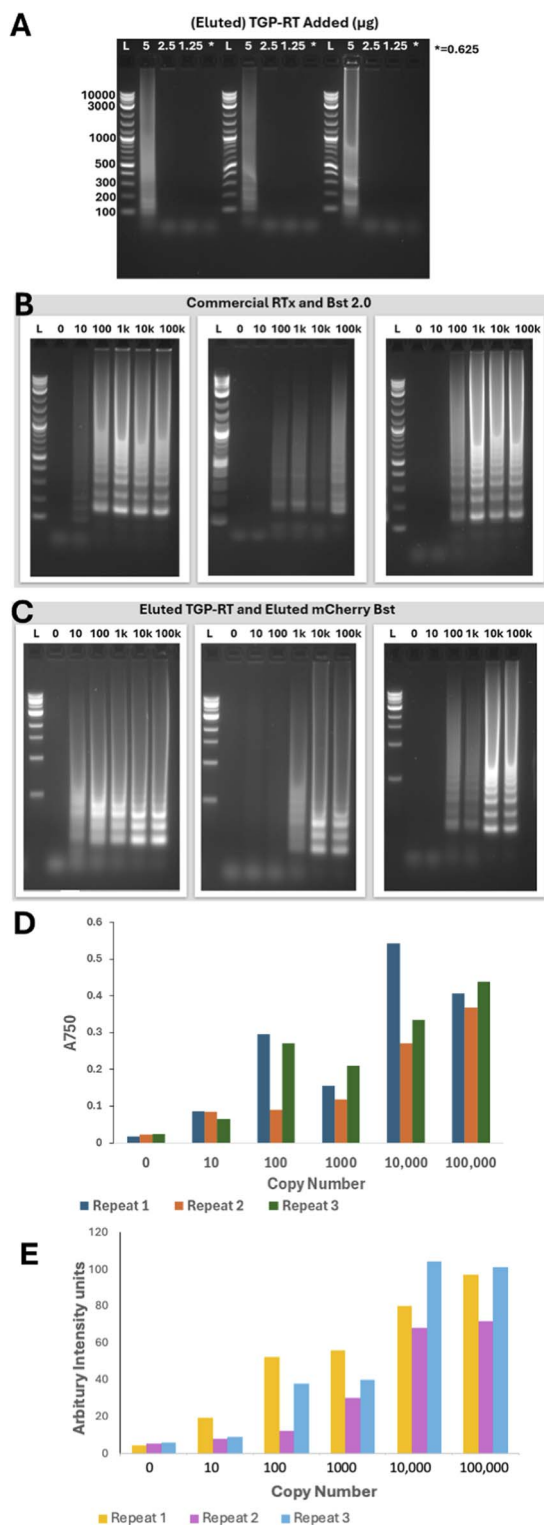
Fig. 8 (A) Effect of eluted TGP-RT concentration on false positive outcome in triplicate using the CAB3 primer set and no template (65 °C for 30 minutes), using 2.5 µg mCherry-Bst and the indicated mass of TGP-RT (5, 2.5, 1.25, or 0.625 µg). NEB 1 kb Plus ladder – 'L' – bands marked. (B) Examples of CAB3 RT-LAMP with RdRp (NS5) DENV S1 RNA template at the indicated starting copy number (0, 10, 100, 1000, 10 000, 100 000 copies), showing variation in output. Reactions utilised commercial NEB Bst 2.0 and RTx. (C) Like B but using silica-eluted mCherry-Bst (2.5 µg) and TGP-RT (2.5 µg). (D) Turbidity analysis for reactions in part C, taking measurement of A750. (E) Intensity scan using Image J of the gel bands in C.

implementing His-purification or other chromatographic techniques, or requiring expensive fluorescent DNA-binding labels.

Conclusions

The aim of this work was to extend the modular fusion protein architecture for NAAT diagnostics[21] to develop a system for virus detection and diagnosis, providing a DENV RT-LAMP diagnostic (Scheme 1) which would be suitable for local production in the Philippines, without specialist protein production facilities or international supply chain dependency. The recombinant architecture (R5-fluorescent protein-functional enzyme) was implemented using an RT enzyme, and TGP (a heat tolerant fluorescent protein), producing TGP-RT, which facilitated both visual distinction and heat-purification at 95 °C. The latter provided high TGP-RT yields.

N-terminal truncation of a 3 amino acids-SSK-from the R5 silica-affinity tag also produced a silaffin variant with improved silica binding efficiency (up to ~60 µg mg^{-1} silica for Δ3R5mCherry-Bst and ~50 µg mg^{-1} silica for Δ3R5-TGP-RT). The silica immobilisation provided both low cost purification and protein stabilisation during storage, enabling both Bst and RT to retain activity for over 3 months, even without −70 °C storage facilities. However, although the enzyme can be used while still on the silica, the presence of silica interferes with turbidity measurements, one of the simplest and lowest cost methods commonly utilised in LAMP product detection. In order to incorporate the NAAT into this simple detection system, L-arginine was used to trigger elution of the enzymes from the silica, so that the soluble enzymes could be used in LAMP without silica interference. The eluted enzymes achieved RT-LAMP for DENV-1 with a detection limit between 10–100 copies.

DENV-1 is more generally widespread than the other serotypes in the Philippines and was recorded in 93% of cases in 2023, showing persistence in endemic outbreaks.[7] A new primer set was designed primarily targeting this serotype. The previously favoured 3′UTR region for primer design was avoided, due to the strong secondary structures in this region, leading to partial complementarily and making it unsuitable for unique LAMP primer sequences, thereby causing a high likelihood of false positives arising.

Instead, the RNA-dependent RNA polymerase (RdRp), part of the NS5 region, was chosen and primer sets evaluated by estimating the free energies of potential dimers. Together with the low resource Bst and RT enzyme production, there is potential for the new CAB3 primer set to aid in the rapid diagnosis of Dengue. This can influence the care pathway and guide appropriate treatment for a virus, with reduction in the use of antibiotics (a first line treatment for febrile disease).

The principles developed and tested within this study and elsewhere in LMICs provides efficient solutions to fundamental bottlenecks in the testing capacities of LMICs, by focussing on sustainable bioreagent production, which has generally been neglected in favour of short-term philanthropy in the supply of diagnostics produced elsewhere. While the model has targeted 'on demand' production with distributed manufacture,

demanding relatively low batch production and avoiding cold chain storage, there is still work required to standardise this simple process as a robust production in less controlled environments. Ongoing regional studies in LMICs have adopted the production processes alongside commercial reagents and thereby extended testing capabilities within limited budgets.

Conflicts of interest

There are no conflicts to declare.

Data availability

Data generated in this study (in the form of electrophoresis gels) are given in the manuscript in their original form. Graphs are generated directly from data collected without additional data manipulation.

Supplementary information: data on protein and primer sequences, modelling studies, including Alphafold confidence scores, Ni-His bind resin purification protocol and calibration graphs. See DOI: https://doi.org/10.1039/d5ay00889a.

Acknowledgements

References

1 World Health Organization (WHO), *Neglected Tropical Diseases*, https://www.who.int/health-topics/neglected-tropical-diseases#tab=tab_1.

2 A. J. Rodríguez-Morales, E. López-Medina, I. Arboleda, J. A. Cardona-Ospina, J. E. Castellanos, Á. A. Faccini-Martínez, E. Gallagher, R. Hanley, P. Lopez, S. Mattar, C. E. Pérez, R. Kastner, H. Reynales, F. Rosso, J. Shen, W. E. Villamil-Gómez and M. Fuquen, *Am. J. Trop. Med. Hyg.*, 2024, **112**(1), 182–188.

3 V. H. Ferreira-de-Lima and T. N. Lima-Camara, *Parasites Vectors*, 2018, **11**, 77.

4 L. H. V. Franklinos, K. E. Jones, D. W. Redding and I. Abubakar, *Lancet Infect. Dis.*, 2019, **19**(9), e302.

5 World Health Organization, *Dengue and Severe Dengue*, https://www.who.int/news-room/fact-sheets/detail/dengue-and-severe-dengue.

6 T. T. Islam, C. Quispe, J. Herrera-Bravo, C. Sarkar, R. Sharma, N. Garg, L. I. Fredes, M. Martorell, M. M. Alshehri, J. Sharifi-Rad, S. D. Daştan, D. Calina, R. Alsafi, S. Alghamdi, G. E. Batiha and N. Cruz-Martins, *BioMed Res. Int.*, 2021, 4224816.

7 M. J. Galarion, B. Schwem, C. Pangilinan, A. Dela Tonga, J. A. Petronio-Santos, E. D. Reyes and R. Destura, *Infect. Genet. Evol.*, 2019, **69**, 134–141.

8 S. Bhatt, P. W. Gething, O. J. Brady, J. P. Messina, A. W. Farlow, C. L. Moyes, J. M. Drake, J. S. Brownstein, A. G. Hoen, O. Sankoh, M. F. Myers, D. B. George, T. Jaenisch, G. R. W. Wint, C. P. Simmons, T. W. Scott, J. J. Farrar and S. I. Hay, *Nature*, 2013, **496**, 504–507.

9 P. Bhatt, S. P. Sabeena, M. Varma and G. Arunkumar, *Curr. Microbiol.*, 2021, **78**, 17–32.

10 S. Das, M. R. Pingle, J. Muñoz-Jordán, M. S. Rundell, S. Rondini, K. Granger, G. J. Chang, E. Kelly, E. G. Spier, D. Larone, E. Spitzer, F. Barany and L. M. Golightly, *J. Clin. Microbiol.*, 2008, **46**(10), 3276–3284.

11 F. Ul Haq, M. Imran, Z. Aslam, F. Mukhtar, K. Jabeen, M. Chaudry, S. U. Rahman and N. Muhammad, *Am. J. Trop. Med. Hyg.*, 2023, **109**(6), 1284–1289.

12 S. D. Blacksell, R. G. Jarman, M. S. Bailey, A. Tananunchitcharnchai, K. Jenjaroen, R. V. Gibbons, D. H. Paris, R. Premaratna, H. J. de Silva, D. G. Lallo and N. P. J. Day, *Clin. Vaccine Immunol.*, 2011, **18**(12), 2095–2101.

13 K. R. Chan, A. A. Ismail, G. Thergarajan, C. S. Raju, H. C. Yam, M. Rishya and S. D. Sekaran, *Front. Cell. Infect. Microbiol.*, 2022, **12**, 975398.

14 K. Jiang, J.-H. Lee, T. S. Fung, J. Wu, C. Liu, H. Mi, R. P. J. Rajapakse, U. B. Balasuriya, Y.-K. Peng and Y. Y. Go, *Anal. Chim. Acta*, 2023, **1274**, 341565.

15 S. Kumar, S. Sharma, N. Bhardwaj, V. Pande, D. Savargaonkar and A. R. Anvikar, *J. Virol. Methods*, 2021, **293**, 114168.

16 C. Henderson, E. Pumford, D. Seevaratnam, R. Daly and E. A. H. Hall, *Biomaterials*, 2019, **193**, 58–70.

17 J. Nkengasong, *Nature*, 2020, **580**, 565.

18 Z. J. Madewell, *South. Med. J.*, 2020, **113**(10), 520–523.

19 P. F. Wong, L. P. Wong and S. AbuBakar, *J. Infect. Public Health*, 2020, **13**(2), 193–198.

20 A. K. Sy, C. Koo, K. J. R. Privaldos, M. A. T. Quinones, M. A. U. Igoy, S. Y. A. M. Villanueva, M. L. Hibberd, L. C. Ng and H. C. Hapuarachchi, *Viruses*, 2023, **15**(5), 1079.

21 D. Seevaratnam, F. Ansah, Y. Aniweh, G. A. Awandare and E. A. H. Hall, *Anal. Bioanal. Chem.*, 2022, **414**(21), 6309–6326.

22 *EDCTP RIA2020EF-2918: - AfriDx Diagnostics Project*, https://afridx.ceb.cam.ac.uk/.

23 M. Xu, M. J. Bailey, J. Look and F. Baneyx, *Protein Expr. Purif.*, 2020, **170**, 105608.

24 M. Kamalov, A. Hajradini, C. Rentenberger and C. F. W. Becker, *Mater. Lett.*, 2018, **212**, 114–117.

25 J. W. Ellefson, J. Gollihar, R. Shroff, H. Shivram, V. R. Iyer and A. D. Ellington, *Science*, 2016, **352**(6293), 1590–1593.

26 D. W. Close, C. D. Paul, P. S. Langan, M. C. J. Wilce, D. A. K. Traore, R. Halfmann, R. C. Rocha, G. S. Waldo, R. J. Payne, J. B. Rucker, M. Prescott and A. R. M. Bradbury, *Proteins*, 2015, **83**(7), 1225–1237.

27 A. J. Milligan and F. M. Morel, *Science*, 2002, **297**(5588), 1848–1850.

28 N. K. Singh, K. Pushpavanam and M. Radhakrishna, *ACS Appl. Bio Mater.*, 2024, **7**(2), 596–608.

29 M. M. Pena, D. Teper, H. Ferreira, N. Wang, K. U. Sato, M. I. T. Ferro and J. A. Ferro, *PLoS One*, 2020, **15**(7), e0236185.

30 S. Hada, U. Burlakoti, K. H. Kim, J. S. Han, M. J. Kim, N. A. Kim and S. H. Jeong, *Int. J. Pharm.*, 2023, **647**, 123545.

31 C. Lange and R. Rudolph, *Curr. Pharm. Biotechnol.*, 2009, **10**(4), 408–414.

32 B. Hellner, S. B. Lee, A. Subramaniam, V. R. Subramanian and F. Baneyx, *Langmuir*, 2019, **35**(14), 5013–5020.

33 T. Teramoto, Y. Kohno, P. Mattoo, L. Markoff, B. Falgout and R. Padmanabhan, *RNA*, 2008, **14**(12), 2645–2656.

34 A. Songjaeng, S. Thiemmeca, D. Mairiang, N. P. K. Kongmanas, P. Hansuealueang, N. Tangthawornchaikul, T. Duangchinda, J. Mongkolsapaya, K. Sriruksa, W. Limpitikul, P. Malasit and P. Avirutnan, *Viruses*, 2022, **14**(6), 1271.

35 E. Alm, B. Lesko, G. Lindegren, C. Ahlm, S. Söderholm, K. I. Falk and N. Lagerqvist, *PLoS Neglected Trop. Dis.*, 2014, **8**(12), e3416.

36 Y. Y. Go, R. P. V. J. Rajapakse, S. A. M. Kularatne, P.-Y. A. Lee, K. B. Ku, S. Nam, P.-H. Chou, Y.-L. Tsai, Y.-L. Liu, H.-F. G. Chang, H.-T. T. Wang and U. B. R. Balasuriya, *J. Clin. Microbiol.*, 2016, **54**(6), 1528–1535.

37 M. Niu, Y. Zhao, L. Chen, J. Wang, X. Li, H. Yang, Q. Zhang and R. Huang, *Front. Immunol.*, 2024, **15**, 1491230.

38 B. Lopez-Jimena, M. Bekaert, M. Bakheit, S. Frischmann, P. Patel, E. Simon-Loriere, L. Lambrechts, V. Duong, P. Dussart, G. Harold, C. Fall, A. A. Sall and M. Weidmann, *PLoS Neglected Trop. Dis.*, 2018, **12**(5), e0006381.